Journal of Engineering and Applied Sciences 2 (10): 1553-1562, 2007
ISSN: 1816-949X

Meso-Mechanical Analysis of 3D Braided Composites Based on a Finite Element Model

Xu Kun and Xu Xiwu
College of Aerospace Engineering, Nanjing University of Aeronautics and Astronautics,
Nanjing 210016, People's Republic of China

Abstract: As for 3D 4-directional rectangular braided composites, a 3-Dimensional (3D) Finite Element Model (FEM) based on a Representative Volume Element (RVE) is established under the periodical displacement boundary conditions, which truly simulates the spatial configuration of the braiding yarns. The FE software ABAQUS is adopted to study the mechanical properties of the composites, including the effective elastic properties and the meso-scale mechanical behaviors. The effects of the braiding angle and the fiber-volume fraction on the engineering elastic constants have been investigated in detail. The predicted effective elastic properties are in good agreement with the available experimental data, demonstrating the applicability of the FEM. By analyzing the stress distribution and deformation of the model, it is proved that the RVE-based FEM can obtain reasonable stress field and successfully represent the meso-scale mechanical behaviors of 3D braided composites containing periodical structures.

Key words: Braided composites, finite element model, effective elastic properties, stress distribution, unit cell

INTRODUCTION

Three-Dimensional (3D) braided composites have been attractive for industrial applications because of their excellent mechanical performances, such as better out-of plane stiffness, strength and high impact resistance, etc, compared with the fiber-reinforced laminated composites. However, due to their complicated architectures and anisotropic nature, it is difficult to predict the mechanical properties of 3D braided composites.

To make full use of 3D braided composites, many models have been developed to analyze the microstructure (Li *et al*., 1990; Du and Ko, 1993; Wang and Wang, 1994; Pandey and Hahn, 1996; Chen *et al*., 1999) and the mechanical properties (Ma *et al*., 1984, 1986; Sun and Sun, 2004; Sun and Qiao, 1997; Gu, 2004; Lei *et al*., 1992; Sun *et al*., 2003; Zeng *et al*., 2004; Tang and Postle, 2002; Chen *et al*., 1999; Yu and Cui, 2007). Ma *et al*. (1984, 1986) studied the effective elastic properties of 3D braided composites by using the 'Fiber interlock model' based on the maximum strain energy principle and the 'Fiber inclination model' based on the modified laminate theory. Wang and Wang adopted a mixed volume averaging technique to predict the mechanical properties of 3D braided composites. Sun and Sun (2004) reported a volume-average-compliance method to calculate the elastic constants. Sun and Qiao (1997) studied the tensile strength based on the modified classical laminate theory. Gu (2004) presented an analytical model to predict the uniaxial tensile strength based on the strain energy conservation law. Lei *et al*. (1992) adopted a 3D truss finite element technique to analyze the mechanical properties of 3D braided composites. Recently, two new prediction models based on finite element procedures (Sun *et al*., 2003; Zeng *et al*., 2001) were developed to evaluate the elastic performance of 3D braided composites. Tang and Postle (2002) analyzed the nonlinear deformation of 3D braided composites by the finite element method. Chen *et al*. (1999) proposed a finite multiphase element method to predict the effective elastic properties. Yu and Cui (2007) developed a two-scale method to predict the mechanics parameters of 3D braided composites.

Although these analytical and computational models have contributed to an enhanced understanding of the mechanical properties of 3D braided composites, the models have their own limitations. For example, simple architectures considered in the analytical models (Ma *et al*., 1984, 1986; Sun and Sun, 2004; Sun and Qiao, 1997) have great difference with the truly geometrical microstructure of 3D braided composites. As the analytical models based on the laminate theory have inherent limitations in geometrical modeling, they are mainly devoted to predicting the global stiffness properties of 3D braided composites. Further, the computational models based on finite element methods

Corresponding Author: Xu Kun, College of Aerospace Engineering, Nanjing University of Aeronautics and Astronautics, Nanjing 210016, People's Republic of China

(Lei *et al*., 1992; Sun *et al*., 2003; Zeng *et al*., 2004; Tang and Postle, 2002) also considered the architectures of the composites to be too simplified and the uniform strain boundary conditions were applied in the periodical unit cell model (Chen *et al*., 1999), which made it difficult to obtain an accurate local stress distribution of 3D braided composites.

In order to predict the mechanical properties of 3D braided composites, it is necessary to establish a model for obtaining the accurate stress distribution of 3D braided composites. However, there are few literatures on predicting the local stress distribution and deformation of 3D braided composites, which is important to accurately predict their mechanical properties. Compared with the analytical models based on the laminate theory, 3D meso-mechanical finite element methods can contribute to truly model the microstructure of 3D braided composites. The main objective of the present work is to develop a new 3D finite element model for obtaining the stress distribution and effective elastic properties of 3D braided composites. The model has taken into account the periodical structure of the composites and the interaction between the braiding yarns. The periodical displacement boundary conditions have been applied in the model. In order to fully exploit the potential of 3D braided composites, the effect of the braiding angle and the fiber-volume fraction on the mechanical properties is analyzed in detail. The predicted effective elastic properties are in good agreement with the available experimental data, demonstrating the applicability of the meso-mechanical FEM. By analyzing the stress distribution and deformation of the model, some conclusions are drawn herein.

MICROSTRUCTURE ANALYSIS AND UNIT CELL MODEL

Although a few representative unit cell geometrical models (Li *et al*., 1990; Du and Ko, 1993; Wang and Way, 1994; Pandey and Hahn, 1996; Chen *et al*., 1999) have been proposed to describe the microstructure of 3D braided composites, some assumptions of these models are apparently unreasonable or too simple. It makes some vital architecture features of the yarn configuration inconsistent with the true microstructure of 3D braided composites. For example, 3D braided composites are composed of the complex fiber-bundle geometry and the matrix pockets. In order to consider the mutual squeeze of the yarns, the cross-section shape of the yarn has usually been supposed to be elliptical. The assumption makes the configuration of the yarns apparently different with the experimental phenomena observed experimentally (Chen *et al*., 1999) which showed that the yarns contacted with each other by sharing a plane due to their mutual squeeze. This important microstructure feature should not be neglected in the geometrical modeling, which greatly influences the stress distribution of 3D braided composites.

In order to perform the analysis of mechanical performances of 3D braided composites successfully, it is important to establish a reasonable microstructure geometrical model which can describe the spatial configuration of the yarns effectively. According to the movement of the yarn carriers on the braiding machine bed and experimental observation (Chen *et al*., 1999) the microstructure of 3D 4-directional braided composites produced by the four-step 1×1 braiding procedure has been investigated in detail.

To ensure consistent and uniform fabric structure, suppose the braiding procedure keep relatively steady, at last in a specified length of braiding. According to the movements of carriers, 3D 4-directional braided composites can be regarded to be made of an infinite of two kinds of repeated sub-cells, A and B. Figure 1 schematically shows the distribution of sub-cell A and sub-cell B in the cross-section of rectangular specimen. As shown in Fig. 1, sub-cell A and sub-cell B are constructed, respectively, based on two braiding yarns in the cross directions. The difference between sub-cell A and sub-cell B is the spatial directions of the braiding yarns. It is noteworthy that sub-cell A and sub-cell B marked with the dash lines distribute alternately every half of a pitch length h in the braiding direction of the z axis, as shown in Fig. 2.

Due to the complicated microstructure of 3D braided materials, it makes unfeasible to undertake a full micromechanical simulation aiming at a whole structure. Instead, Representative Volume Element (RVE)-based approach can be used to analyze the mechanical properties in the macro-meso scales. Considering the periodical feature of sub-cell distribution, a unit cell that is the smallest periodical RVE is selected as shown in Fig. 1. According to the unit cell partition scheme, all the unit cells are oriented in the same reference frame as the specimen, which is quite favorable for the analysis of the mechanical properties. Figure 2 shows the topological relation of the main yarns in a parallelepiped unit cell. γ is the angle between the central axis of the braiding yarn and the *z*-axis. The relationship between the angle γ and the surface braiding angle α, is defined as

$$\tan\gamma = \sqrt{2}\tan\alpha \quad (1)$$

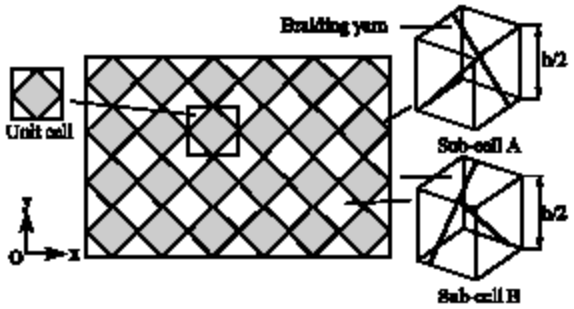

Fig. 1: Distribution of unit cells on the cross-section of rectangular specimen

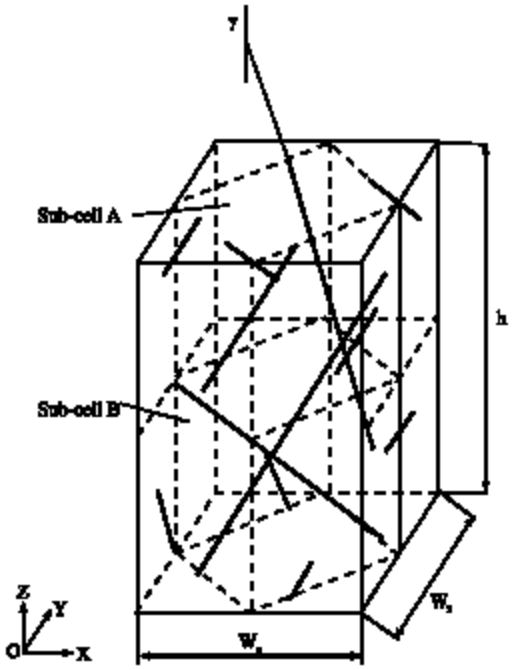

Fig. 2: Topological relation of the main yarns in the unit

The solid unit cell model of 3D 4-directional braided composites is shown in Fig. 3. All the yarns used in the braided performs are assumed to have the same constituent material, size and flexibility. Considering the mutual squeezing of the yarns, the cross-section shape of the braiding yarn perpendicular to the central axis is assumed to be octagonal and the octagon contains an inscribed ellipse with major and minor radii, a and b, respectively, which is shown in Fig. 4.

The width and the pitch length of the unit cell are, respectively

$$W_x = W_y = 4\sqrt{2}b \tag{2}$$

and

$$h = \frac{8b}{\tan\gamma} \tag{3}$$

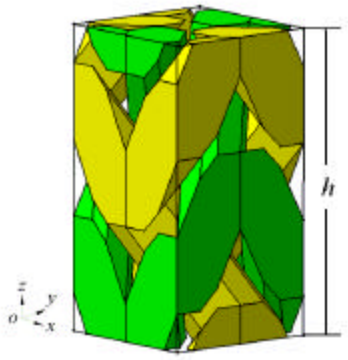

Fig. 3: Yarn configuration of the solid unit cell

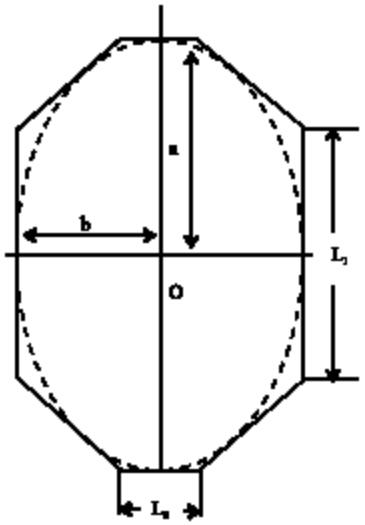

Fig. 4: Cross-section shape of yarn

According to the tangent relationship of the elliptical-cylinders of the braiding yarns, the relationship between the major and minor radii of the inscribed ellipse, a and b, can be obtained:

$$a = \sqrt{3}b\cos\gamma \tag{4}$$

The lengths of L_1 and L_2 in Fig. 4, are given by:

$$L_1 = 2\left[\sqrt{b^2\cot^2\gamma + \frac{a^2}{\sin^2\gamma}} - b\cot\gamma\right]\sin\gamma \tag{5}$$

$$L_2 = 2\left[\sqrt{b^2\cot^2\gamma + \frac{a^2}{\sin^2\gamma}}\right]\sin\gamma \tag{6}$$

As the idealized braided composites considered herein are assumed to be made of the repeated unit cells, the fiber volume fraction of 3D braided composites can be determined by the following expression:

$$V_f = \frac{V_y}{V_u}\varphi \tag{7}$$

Where, V_y is the volume of all the yarns in the unit cell, V_u is the volume of the whole unit cell and φ is the fiber volume fraction of the yarn.

The 3D solid unit cell can be established by using the CAD/CAM software CATIA P3 V5R14.

FINITE ELEMENT MODEL

The RVE-based meso-mechanical FEM mainly consists of three parts: The periodical boundary conditions and finite element meshing, the constitutive relations of components and the definition of the effective elastic properties. The details of the finite element model are presented in the subsections.

Periodical displacement boundary conditions and finite element meshing: Since the analysis is based on the RVE, the periodical boundary conditions should be applied in the model in order to obtain a reasonable stress distribution. Two continuities must be satisfied at the boundary surfaces of the neighboring cubic RVEs. The first is that the displacements must be continuous, and the second is that the traction distribution at the opposite parallel boundaries of the RVE must be uniform. Therefore, the unified periodical displacement boundary conditions suitable for the RVE proposed by Xia *et al.* (2003) were employed in the model. These general formulas of the boundary conditions are given as follows:

$$u_i = \bar{\varepsilon}_{ik} x_k + u_i^* \tag{8}$$

$$u_i^{j+} = \bar{\varepsilon}_{ik} x_k^{j+} + u_i^* \tag{9}$$

$$u_i^{j-} = \bar{\varepsilon}_{ik} x_k^{j-} + u_i^* \tag{10}$$

$$u_i^{j+} - u_i^{j-} = \bar{\varepsilon}_{ik}(x_k^{j+} - x_k^{j-}) = \bar{\varepsilon}_{ik}\Delta x_k^j \tag{11}$$

In Eq. 8, $\bar{\varepsilon}_{ik}$ is the global average strain tensor of the periodical structure, μ_i^* is the periodic part of the displacement components on the boundary surfaces and it is generally unknown. For a cubic RVE as shown in Fig. 4, the displacements on a pair of opposite boundary surfaces (with their normals along the X_j axis) are expressed as in Eq. 9 and 10, in which the index "j+" means along the positive X_j direction and "j-" means along the negative X_j direction. The difference between Eq. 9 and 10 is given in Eq. 11. Since Δ^j_k are constants for each pair of the parallel boundary surfaces, with specified $\bar{\varepsilon}_{ik}$, the right side of Eq. 11 become constants.

It can be seen that Eq. 11 does not contain the periodic part of the displacement. It becomes easier to apply the nodal displacement constraint equations in the finite element procedure, instead of giving Eq. 8 directly as the boundary conditions. In order to apply the constraint Eq. 11 in the FEM, the same meshing at each two paired boundary surfaces of the RVE should be produced.

Due to the complexity of the microstructure the 3D solid tetrahedron elements were applied to mesh the whole model, as shown in Fig. 5. The model is composed of the straight yarns in various directions and the matrix pocket from Fig. 5. It is assumed that the perfect bonding exists between the yarns and the resin matrix pocket. Uniform meshes had been made to satisfy the continuities of stress and displacement on the interfaces of the constitutive materials, including the interfaces of the yarns in different directions and the interfaces between the yarns and the resin matrix pocket.

Constitutive relations of components: As shown in Fig. 5, two "types" of materials are contained in the model. They are the yarns and the resin matrix pocket, respectively. The yarns can generally be regarded as the unidirectional fiber-reinforced composites in the material coordinates systems. The principal direction 1 of the material coordinates systems for a yarn is defined to be paralleled with the fiber direction. The yarns and the resin matrix pocket are assumed to be transversely isotropic and isotropic, respectively. Both of them are believed to be linearly elastic in the model. The engineering elastic constants of the yarn can be calculated by the famous micromechanics formulae proposed by Chamis (1989):

$$\begin{aligned}
&E_1 = \varphi E_{f1} + (1-\varphi)E_m,\\
&E_2 = E_3 = \frac{E_m}{1-\sqrt{\varphi}(1-E_m/E_{f2})},\\
&G_{12} = G_{31} = \frac{G_m}{1-\sqrt{\varphi}(1-G_m/G_{f12})},\\
&G_{23} = \frac{G_m}{1-\sqrt{\varphi}(1-G_m/G_{f23})},\\
&\nu_{12} = \nu_{13} = \varphi\cdot\nu_{f12} + (1-\varphi)\nu_m,\\
&\nu_{23} = \frac{E_2}{2G_{23}} - 1.
\end{aligned} \tag{12}$$

Where, φ is the fiber volume fraction of the yarn, E_{f1} is the Young's elastic modulus of the fiber in principle axis *1*, E_{f2} is the Young's elastic modulus of the fiber in

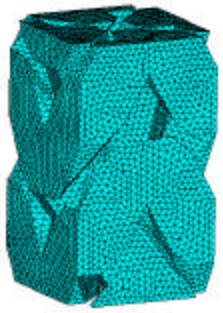

(a) Yarns

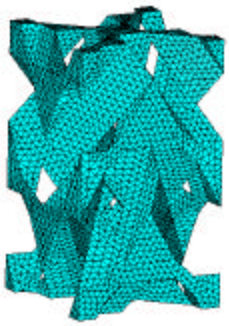

(b) Resin matrix pocket

Fig. 5: Finite element mesh of the model

principle axis 2, G_{f12} is the longitudinal shear modulus of the fiber, G_{f23} is the transverse shear modulus of the fiber, v_{f12} is the primary Poisson's ratio of the fiber, E_m, V_m and $G_m(G_m = E_m/2(1 + v_m))$ represent the Young's elastic modulus, Poisson's ratio and shear modulus of the matrix, respectively.

Effective elastic properties: To obtain the effective elastic properties of 3D 4-directional braided composites, a homogenization approach is employed in this study by considering the heterogeneous composites in the micro-scale to be a homogeneous material in the macro-scale. Given the periodic cubic RVE, the global strain-global stress relation can be written as

$$\bar{\varepsilon}_i = S_{ij}\bar{\sigma}_j \tag{13}$$

Where, S_{ij} is the effective compliance matrix. Assuming a set of the global strain, $\bar{\varepsilon}_{ik}$ and applying the periodic boundary conditions in the form of Eq. 11 in the FEM analysis, we can obtain a unique stress distribution of the RVE. Then the global stress, $\bar{\sigma}_{ik}$, corresponding to this set of global strains can be obtained by

$$\bar{\sigma}_{ik} = \frac{1}{V}\int_V \sigma_{ik}\,dV \tag{14}$$

In the 3D case applying this set of $\bar{\varepsilon}_{ik}$ (six components), six equations thus can be obtained. For a general case where there is no orthotropic axis of symmetry of the material, the application of four linearly independent sets of the global strains $\bar{\varepsilon}_{ik}$ will have sufficient equations to determine 21 independent material constants of the compliance matrix S_{ij} (Xia *et al*., 2003).

As the effective compliance matrix S_{ij} is one of the inherent properties for 3D braided materials with the decided microstructure and component materials, the calculation of its value has on relation with the boundary conditions applied on the RVE. To avoid the trouble of solving the equations, six sets of global strains were applied in the FE analysis of RVE. Six sets of loading case of periodical displacement boundary conditions are shown in Table 1.

Table 1: Loading cases of periodical displacement boundary conditions

k	$\bar{\varepsilon}_x$	$\bar{\varepsilon}_y$	$\bar{\varepsilon}_z$	$\bar{\gamma}_{yz}$	$\bar{\gamma}_{xz}$	$\bar{\gamma}_{xy}$
1	0.01	0	0	0	0	0
2	0	0.01	0	0	0	0
3	0	0	0.01	0	0	0
4	0	0	0	0.02	0	0
5	0	0	0	0	0.02	0
6	0	0	0	0	0	0.02

By prescribing the six sets of the global strains, $\bar{\varepsilon}_{ik}^{k}$ (k = 1,2..6), the corresponding global stress $\bar{\sigma}_{ik}^{k}$ can be calculated by Eq. 14. Then the following equations can be obtained

$$\left(\bar{\varepsilon}_{i1}^{1}, \bar{\varepsilon}_{i1}^{2}, \ldots, \bar{\varepsilon}_{i1}^{5}, \bar{\varepsilon}_{i1}^{6}\right) = S_{ij}\left(\bar{\sigma}_{i1}^{1}, \bar{\sigma}_{i1}^{2}, \ldots, \bar{\sigma}_{i1}^{5}, \bar{\sigma}_{i1}^{6}\right) \tag{15}$$

It is easy to obtain the effective compliance matrix S_{ij} through

$$S_{ij} = \left(\bar{\varepsilon}_{i1}^{1}, \bar{\varepsilon}_{i1}^{2}, \ldots, \bar{\varepsilon}_{i1}^{5}, \bar{\varepsilon}_{i1}^{6}\right)\left(\bar{\sigma}_{i1}^{1}, \bar{\sigma}_{i1}^{2}, \ldots, \bar{\sigma}_{i1}^{5}, \bar{\sigma}_{i1}^{6}\right)^{-1} \tag{16}$$

RESULTS AND DISCUSSION

Comparison of effective elastic properties with experimental results: In order to verify the applicability of the FEM based on the software ABAQUS, three examples with typical braiding angles are selected from the available experiments studied by Chen *et al*. (1999). All the analyses reported herein were done for the 3D 4-directional braided composites by the 4-step 1×1 rectangular braiding procedures. The elastic properties of

Table 2: Mechanical properties of component materials

Materials	E_{f1} (GPa)	E_{f2} (GPa)	G_{f12} (GPa)	G_{f23} (GPa)	v_{f12}	v_m
Carbon fiber T300	230	40	24	14.3	0.25	
Epoxy resin	3.5					0.35

Table 3: Braiding parameters of specimens and structural parameters of unit cell model

	Braiding parameters of specimens			Structural parameters of unit cell model					
No.	Dimensions (mm)	α(°)	V_f(%)	γ(°)	a(mm)	b(mm)	φ(%)	$W_x = W_y$ (mm)	h (mm)
1	20×6×250	19.0	46.6	26.0	0.599	0.385	57.8	2.175	6.317
2	20×6×250	30.0	47.2	39.2	0.542	0.404	60.7	2.286	3.960
3	20×6×250	37.0	47.1	46.8	0.503	0.425	62.3	2.402	3.188

the component materials, including 12K T300 carbon fiber and TDE-85 epoxy resin, are listed in Table 2. According to the braiding process parameters of three specimens from Chen *et al*. (1999) the main microstructure parameters of unit cell models used in the calculation is shown in Table 3.

According to the meshing scheme of the FEM, adaptive finite element meshes were used to keep element size small in the edges of the matrix pocket. In the study, the FEM for specimen No.1 consists of 9854 nodes and 49030 tetrahedron elements. The FEM for specimen No.2 consists of 17462 nodes and 88700 tetrahedron elements, the FEM for specimen No.3 consists of 15298 nodes and 78518 tetrahedron elements. It is noted that relatively fine meshing size is required in order to obtain more accurate stress distribution, especially near the boundaries of the RVE. However, if only the global stiffness is concerned, relative coarse meshing size can still provide satisfactory results (Xia *et al*., 2006). The meshing size of the models in this study is sufficient to guarantee the convergence of the solutions.

The effective elastic properties of 3D braided composites are first calculated by the FEM and the calculated stiffness properties are compared with Chen *et al*. (1999). The effective compliance matrix S_{ij} for specimen No.1, 2 and 3 are given, respectively, as follows:

$$S_{ij} = \begin{bmatrix} 0.1208 & -0.0425 & -0.0126 & 0 & 0 & 0 \\ -0.0425 & 0.1208 & -0.0126 & 0 & 0 & 0 \\ -0.0126 & -0.0126 & 0.0182 & 0 & 0 & 0 \\ 0 & 0 & 0 & 0.0965 & 0 & 0 \\ 0 & 0 & 0 & 0 & 0.0965 & 0 \\ 0 & 0 & 0 & 0 & 0 & 0.2535 \end{bmatrix} \times 10^{-3}\ 1/\text{MPa},$$

$$S_{ij} = \begin{bmatrix} 0.1173 & -0.0352 & -0.0284 & 0 & 0 & 0 \\ -0.0352 & 0.1173 & -0.0284 & 0 & 0 & 0 \\ -0.0284 & -0.0284 & 0.0415 & 0 & 0 & 0 \\ 0 & 0 & 0 & 0.0676 & 0 & 0 \\ 0 & 0 & 0 & 0 & 0.0676 & 0 \\ 0 & 0 & 0 & 0 & 0 & 0.1412 \end{bmatrix} \times 10^{-3}\ 1/\text{MPa}$$

and

$$S_{ij} = \begin{bmatrix} 0.1110 & -0.0340 & -0.0388 & 0 & 0 & 0 \\ -0.0340 & 0.1110 & -0.0388 & 0 & 0 & 0 \\ -0.0388 & -0.0388 & 0.0624 & 0 & 0 & 0 \\ 0 & 0 & 0 & 0.0642 & 0 & 0 \\ 0 & 0 & 0 & 0 & 0.0642 & 0 \\ 0 & 0 & 0 & 0 & 0 & 0.0973 \end{bmatrix} \times 10^{-3}\ 1/\text{MPa}$$

It is found that 3D 4-directional braided composites can be considered to be transversely isotropic materials in the macro-scale under small deformation assumption. According to the relationship between the engineering elastic constants and the compliance matrix S_{ij}, the engineering elastic constants of 3D 4-directional braided composites, including nine independent elastic constants, can be calculated by

$$\begin{cases} E_x = \dfrac{1}{S_{11}}, \quad E_y = \dfrac{1}{S_{22}}, \quad E_z = \dfrac{1}{S_{33}} \\ \mu_{xy} = -\dfrac{S_{12}}{S_{22}}, \quad \mu_{xz} = -\dfrac{S_{13}}{S_{33}}, \quad \mu_{yz} = -\dfrac{S_{23}}{S_{33}} \\ G_{yz} = \dfrac{1}{S_{44}}, \quad G_{xz} = \dfrac{1}{S_{55}}, \quad G_{xy} = \dfrac{1}{S_{66}} \end{cases} \tag{17}$$

Table 4 gives the predicted and measured elastic constants of 3D braided composite. There is a good agreement between the measured and predicted axial tensile modulus for all the three samples studied. The predicted Poisson' ratios are basically agreed with the measured values. The results indicate that the proposed FEM can be used to calculate the global elastic properties, demonstrating the applicability of the meso-mechanical FEM.

Deformation of unit cell and distribution of stress: For 3D 4-directional braided composites with periodical structures, RVE-based finite element model can also be used to calculate the mechanical properties in the meso-scale, such as the deformation of the model, distribution

Table 4: Comparison of the effective elastic constants predicted by the model and experimental data

	No.1		No.2		No.3	
Elastic constants	Experiment	Predicted	Experiment	Predicted	Experiment	Predicted
E_x/GPa		8.28		8.52		9.01
E_y/GPa		8.28		8.52		9.01
E_z/GPa	58.74	54.85	27.60	24.12	18.05	16.03
G_{xz}/GPa		10.36		14.80		15.57
G_{yz}/GPa		10.36		14.80		15.57
G_{xy}/GPa		3.95		7.08		10.27
V_{xz}	0.72	0.69	0.78	0.68	0.80	0.62
V_{yz}	0.69	0.69	1.00	0.68	0.72	0.62
V_{xy}		0.35		0.30		0.31

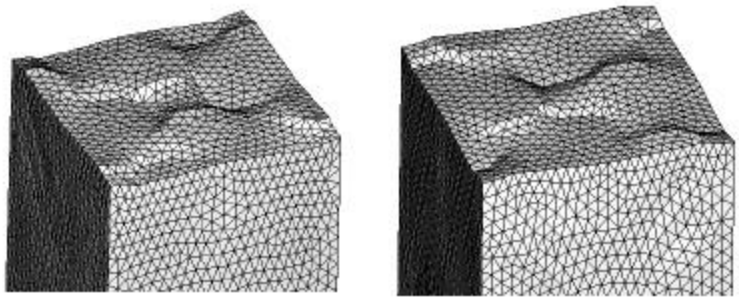

(a) Deformation of positive surface vertical to *z* axis

(b) Deformation of negative surface vertical to *z* axis

Fig. 6: Surface deformation of the model under loading case 3

of stress and stress concentration, etc. To demonstrate the application, the FEM of specimen No.2 subjected to typical loading cases is chosen to show the meso-mechanical behavior of 3D 4-directional braided composites.

Figure 6 shows the deformation of two parallel boundary surfaces vertical to the z axis of the model subjected to loading case 3, k = 3. Under such loading case, $\bar{\varepsilon}_{z}$ equals to 0.01 and all the other 5 effective average strains equal to zero. From Fig. 6, the two opposite boundary surfaces do not remain plane anymore and are warped after the deformation (the magnified factor of the deformation is 100 times). The warped deformation occurs simultaneously at the other two sets of opposite boundary surfaces of unit cell, but the warped extent is relatively weak. The reason resulted in the phenomena is that the unit cell model of 3D 4-directional braided composites does not have the symmetries of geometrical structure and physical properties.

Figure 7 shows the deformation of the model subjected to loading case 6, k = 6. Under such loading case, $\bar{\gamma}_{x}$ equals to 0.02 and all the other five effective average strains equal to zero. From Fig. 7, the set of opposite boundary surfaces vertical to the x axis, respectively, do not remain plane after deformation and the warped deformation has occurred (the magnified factor of the deformation is 50 times). The same warped deformation occurs simultaneously at the opposite boundary surfaces vertical to the y axis. However, the warped deformation extent at the opposite boundary surfaces vertical to the z axis is relatively weak. From Fig. 6 and 7, the FEM based on the periodical displacement boundary conditions guarantees the displacement continuity at the opposite surfaces between the neighboring RVEs.

By analyzing the numerical results of the model, all the stress components at the corresponding parallel boundary surfaces have the uniform stress distribution. For example, Fig. 8 shows the maximum principal stress nephogram of the whole FEM, the yarns and the resin matrix pocket in the model subjected to loading case 3. The traction continuity at the corresponding parallel boundary surfaces has been guaranteed and satisfied the periodic condition. From Fig. 8, it can be seen that the stress in yarns is about 20 times than that in the matrix pocket region. This indicates that the yarns of 3D 4-directional braided composites share the primary tensile load. As shown in Fig. 8 c, stress concentration is produced in the contacting region between the yarns and the matrix pocket. The closer to this region, the greater stress is produced.

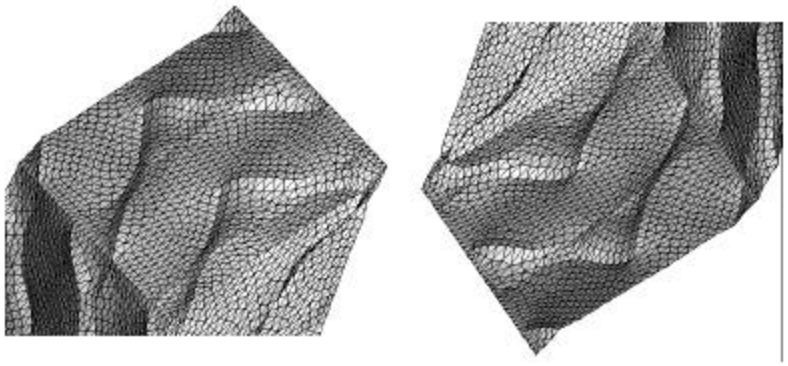

(a) Deformation of positive suface vertical to *x* axis

(b) Deformation of negative suface vertical to *x* axis

Fig. 7: Deformation of the model under loading case 6

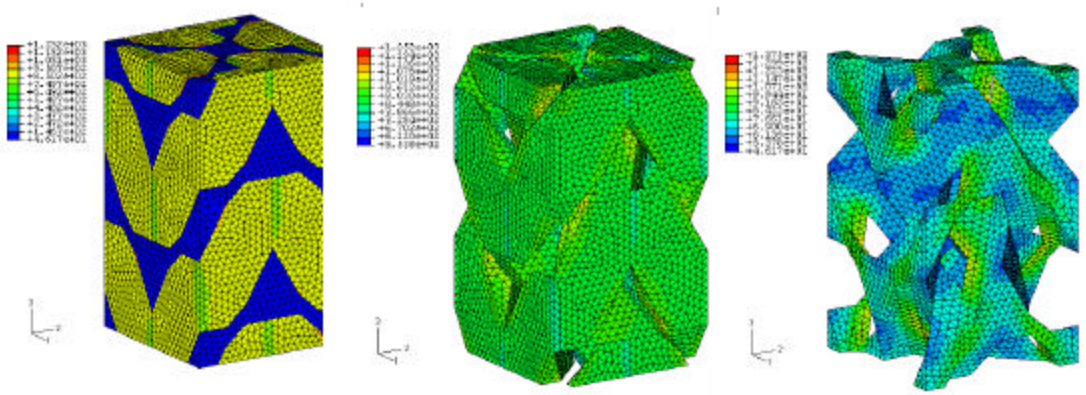

(c) Resin matrix

Fig. 8: Maximal principal stress nephogram of the model No.2 under loadind case 3

Discussion on the effective properties of 3D braided composites: The unit cell of 3D 4-directional braided composites produced by the 4-step 1×1 rectangular braiding procedures can be characterized by two independent micro-structural parameters, including the braiding angle and the fiber-volume fraction. In this section, the effects of the two parameters on the effective elastic properties of 3D braided composites are studied with the meso-mechanical FEM. The models were established as shown in this study. The width of unit cell W_x is assumed to be 2.30 mm in the models. The models with different fiber-volume fractions under a same braiding angle are obtained by defining the fiber-volume fraction of the yarn from Eq. 7. The elastic properties of fibers and matrix are shown in Table 2.

Figure 9 shows the variation of the predicted elastic constants of 3D braided composites with the increasing braiding angle, including three samples with different fiber-volume fractions. Figure 9 a describes that the elastic modulus E_z decreases sharply as the braiding angle increases. With the fiber-volume fraction increasing, the elastic modulus E_z increases as a whole. However, when the braiding angle is small, the change of the elastic modulus E_z caused by the increment of fiber-volume fraction becomes comparatively significant. Figure 9 b gives that the elastic modulus, E_x or E_y ($E_x = E_y$), varies with the braiding angle. The elastic modulus E_x increases steadily as the braiding angle increases. With the fiber-volume fraction increasing, the elastic modulus E_x increases in a similar tendency. Figure 9 c depicts that the shear modulus G_{xy} increases monotonically with the increasing braiding angle. As the fiber-volume fraction increases, the shear modulus G_{xy} increases. When the braiding angle is about 40 deg., the change of the shear modulus G_{xy} caused by the increment of the fiber-volume fraction is comparatively larger with increasing the fiber-

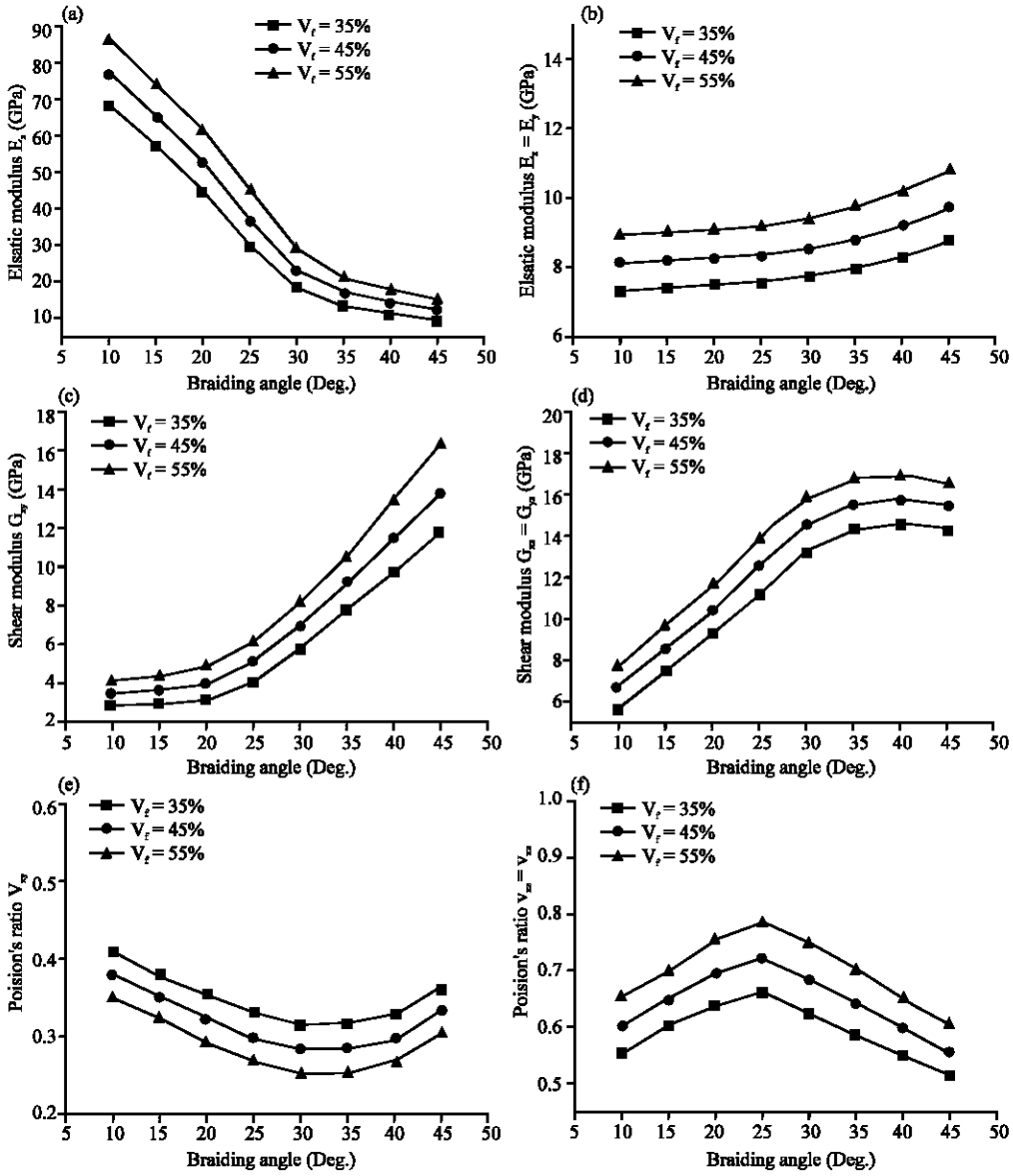

Fig. 9: Variation of engineering elastic constants with structural parameters

olume fraction. Figure 9 d presents that the shear modulus, G_{xz} or G_{yz} ($G_{xz} = G_{yz}$), firstly increases and then decreases. With the increase of the fiber-volume fraction, the shear moduli, G_{xz} and G_{yz}, increase. Figure 9 e-f shows that the variation of the Poison's ratios, v_{xy} and v_{xz} ($v_{xz} = v_{yz}$), with the braiding angle. With increasing the braiding angle, v_{xy} firstly decreases and then increases; v_{xz} and v_{yz} firstly increase and then decrease. As the fiber-volume fraction increases, the Poison's ratio v_{xy} decreases. With increasing the fiber-volume fraction, the Poison's ratios, v_{xz} and v_{yz}, increase.

As shown in Fig. 9, the effective elastic properties of the composites have been influenced by the two structural parameters. Therefore, optimization of the structural parameters can help to reduce the design time and save the manufacture costs.

CONCLUSION

A new finite element model based on the RVE is proposed to predict the effective elastic properties and the meso-mechanical behaviors of 3D braided composites. The 3D model takes into amount the periodical structure of the composites and the interaction between braiding yarns. The predicted effective elastic properties are compared favorably with the experimental data,

demonstrating the applicability of the meso-mechanical FEM. Meanwhile, the method proposed is convenient to predict the effective global stiffness of 3D braided composites. The effect of the braiding angle and fiber-volume fraction on the engineering elastic constants has been discussed in detail. The results show that the elastic modulus E_{zy} is influenced significantly by the braiding angle. By analyzing the stress distribution and deformation, it is proved that the model guarantees the displacement continuity and the traction continuity at the surface boundaries of the neighboring RVEs. The RVE-based finite element model can obtain a reasonable stress field in the meso-scale.

Future research will focus on the strength and failure analysis of 3D 4-directional braided composites by using the meso-mechanical FEM.

ACKNOWLEDGEMENT

This study is financially supported by Postgraduate Innovation Project of Jiangsu Province of China (NO. 2005065). And the authors would like to acknowledge the support given by Postgraduate Innovation Fundation of Nanjing University of Aeronautics and Astronautics (NO.BCXJ05-03).

REFERENCES

Chamis, C.C., 1989. Mechanics of Composites Materials: Past, Present and Future. J. Compos. Tech. Res., 11: 3-14.

Chen, L., Tao, X.M. and C.L. Choy, 1999. On the Microstructure of Three-Dimensional Braided Preforms. Compos. Sci. Tech., 59: 391-404.

Chen, L., X.M. Tao and C.L. Choy, 1999. Mechanical Analysis of 3-D Braided Composites by the Finite Multiphase Element Method. Compos. Sci. Tech., 59: 2383-2391.

Du, G.W. and F.K. Ko, 1993. Unit Cell Geometry of 3-D Braided Structure. J. Reinforced Plastics Compos., 12: 752-768.

Gu, B.H., 2004. Prediction of the Uniaxial Tensile Curve of 4-Step 3-Dimensional Braided Preform. Compos. Struct., 64: 235-241.

Lei, C., Y.J. Cai and F.K. Ko, 1992. Finite Element Analysis of 3-D Braided Composites, In: Advances in engineering solfware. Elsvier Sci. Pub., pp: 187-94.

Li, W., M. Hammad and S.A. El, 1990. Structural Bnalysis of 3-D Braided Preforms for Composites. J. Text Inst. 81: 491-514.

Ma, C.L., J.M. Yang and T.W. Chou, 1984. Elastic Stiffness of Three-Dimensional Braided Textile Structural Composites, Composite Materials: Testing and Design. Seven Conf., pp: 404-421.

Pandey, R. and H.T. Hahn, 1996. Visualization of Representative Volume Elements for Three-Dimensional Four-Step Braided Composites. Compos. Sci. Tech., 56: 161-170.

Sun, H.Y. and X. Qiao, 1997. Prediction of the Mechanical Properties of Three-Dimensionally Braided Composites. Compos. Sci. Tech., 57: 623-629.

Sun, H.Y., S.L. Di and N. Zhang, 2003. Micromechanics of Braided Composites via Multivariable FEM. Comput. Struct., 81: 2021-2027.

Sun, X.K. and C.J. Sun, 2004. Mechanical Properties of Three-Dimensional Braided Composites. Compos. Struct., 65: 485-492.

Tang, Z.X. and R. Postle, 2002. Mechanics of Three-Dimensional Braided Structures for Composite Materials-Part 3: Nonlinear Finite Element Deformation Analysis. Compos. Struct., 55: 307-317.

Wang, Y.Q. and A.S.D. Wang, 1994. On the Topological Yarn Structure of 3-D Rectangular and Tubular Braided Preforms. Compos Sci. Tech., 51: 575-86.

Xia, Z.H., C.W. Zhou and Q.L. Yong, 2006. On Selection of Repeated Unit Cell Model and Application of Unified Periodic Boundary Conditions in Micro-Mechanical Analysis of Composites. Int. J. Solids and Struct., 43: 266-278.

Xia, Z.H., Y.F. Zhang and F. Ellyin, 2003. A Unified Periodical Boundary Conditions for Representative Volume Elements of Composites and Applications. Int. J. Solids Struct., 40: 1907-1921.

Yang, J.M., C.L. Ma and T.W. Chou, 1986. Fiber Inclination Model of Three-Dimensional Textile Structural Composites. J. Compos Mater., 20: 472-483.

Yu, X.G. and J.Z. Cui, 2007. The prediction on mechanical properties of 4-step braided composites via two-scale method. Compos. Sci. Tech., 67: 471-480.

Zeng, T., L.Z. Wu and L.C. Guo, 2004. Mechanical Analysis of 3D Braided Composites: A Finite Element Model. Compos. Struct., 64: 399-404.